Jurnal Polimesin
Department of Mechanical Engineering
State Polytechnic of Lhokseumawe
http://e-jurnal.pnl.ac.id/polimesin
e-ISSN : 2549-1999 No. : 5 Month : October
p-ISSN : 1693-5462 Volume : 23 Year : 2025

Processing dates: received on 2025-08-28, reviewed on 2025-10-23, accepted on 2025-10-26 and online availability on 2025-10-31

Identifying key parameters affecting the mechanical properties of 3D-printed ABS materials

Muhammad Nuzan Rizki[1,*], Reza Putra[1], Alpaslan Durmuş[2], Muhammad Isra[3]
[1]Department of Mechanical Engineering, University of Malikussaleh, Lhokseumawe 24353, Indonesia
[2]Department of Unmanned Aerial Vehicles and Operatorship, OSTİM Technical University, Ankara 06374, Türkiye
[3]Department of Mechanical Engineering, University of Samudra, Langsa, 24416, Indonesia
*Corresponding Author: mnuzanrizki@unimal.ac.id

Abstract

Advances in Additive Manufacturing (AM) technology have enabled the rapid and precise production of complex components, including those used in Unmanned Aerial Vehicle (UAV) structures. However, Acrylonitrile-Butadiene-Styrene (ABS) material prints often exhibit variations in quality due to the influence of various interacting process parameters. This study aims to analyze the impact of four parameters: infill pattern, layer thickness, print speed, and chamber temperature on two important mechanical properties: Ultimate Tensile Strength (UTS) and elongation. The Taguchi method, using an L9(3^4) orthogonal array, was applied to minimize the number of trials while preserving important information. The tensile test data were analyzed using the signal-to-noise ratio (S/N ratio) and Analysis of Variance (ANOVA). The results showed that the infill pattern was the most dominant parameter, accounting for 80.78% of UTS and 73.16% of elongation. Chamber temperature has a significant effect on elongation (19.78%), as it enhances interlayer bonding by controlling temperature in the printing chamber. Layer thickness contributes moderately to UTS (10.01%), while print speed has the least negligible effect on both responses. These findings emphasize the importance of selecting the appropriate parameter combination to consistently improve ABS print quality and serve as a foundation for developing process standards based on experimental data.

Keywords:
3D-printing, Acrylonitrile Butadiene Styrene (ABS), printing parameters, mechanical properties, Taguchi method

1 Introduction

Nowadays, the idea of a manufacturing method capable of producing almost any shape has garnered considerable attention in the design of parts for Unmanned Aerial Vehicles (UAVs). Designing and manufacturing prototypes with complex shapes, parameters, and functions can be a significant challenge when the only manufacturing option is the conventional approach. Additive Manufacturing (AM) technology has become widely popular in addressing these challenges. Its primary advantage lies in its ability to produce complex geometries with relatively low time and cost requirements [1], [2]. Especially nowadays, UAV or drone systems attract significant interest across different sectors due to their flexibility for various purposes and their low operating costs. UAVs can be broadly defined as autonomous, semi-autonomous, or ground-based aircraft that lack a pilot and can be controlled wirelessly using various communication protocols [3][4]. UAVs come in various sizes, shapes, and weights depending on their purpose and capabilities. These aircraft are classified by mission altitude, weight, or wing type.

For civilian UAVs, wing type is the most common classification. UAVs can be classified as fixed-wing, rotary-wing, or hybrid depending on their wing structure. Endurance is the most critical factor in UAV systems [5-7]. Takeoff weight is the most critical parameter affecting endurance. To reduce takeoff weight, lightweight and durable materials must be used in UAV systems. Today, UAVs and drones have more complex airframes to enhance aerodynamics and allow attachment of components, such as cameras, to the airframe. Mold injection and machining, which are conventional manufacturing techniques widely used in UAV and drone production, can increase costs in terms of time and cost [7-9]. Furthermore, creating complex structures using traditional methods is a significant challenge. Furthermore, conventional manufacturing methods increase raw material costs and the crucial takeoff weight of UAVs.

In recent years, 3D printing technology has become widely used in the production of UAV components. Thermoplastic printing materials and their derivatives used in 3D printing technologies play a significant role in reducing production costs and airframe weight [10][11]. Thermoplastic printing materials are much lighter and easier to process than the metals commonly used in traditional manufacturing [12].

UAV structures are generally required to have good strength and reliability. However, the strength-to-weight ratio is an essential key focus. Acrylonitrile-Butadiene-Styrene (ABS) is often used and considered one of the best options. ABS offers ease of 3D printing, affordability, and sufficient mechanical properties for UAV applications, particularly when mechanical loads are not excessively high. Compared to PLA, for example, ABS offers better impact and temperature resistance, though it is often stiffer. Previous research has also highlighted the importance of structural design (e.g., sandwich or honeycomb) to maximize the performance of ABS material [3–6]. Overall, ABS is a popular and viable choice for small UAVs.

However, the final ABS product is strongly influenced by the 3D printing process parameters. One of the main issues in 3D printing with ABS is the high variability in print quality, which is directly influenced by the complexity of the process parameters. Unlike conventional manufacturing processes, which tend to be stable, 3D printing is highly sensitive to changes in printing parameters. Parameters such as nozzle temperature, bed temperature, printing speed, layer height, infill density, infill pattern, chamber temperature, and printing orientation can affect layer bonding and the material's internal structure. For example, a nozzle temperature that is too low can cause weak interlayer bonding, while a printing speed that is too high can result in premature cooling and dimensional defects [7–10].

Infill pattern is undoubtedly one of the most influential factors. Each type of infill pattern has a different internal structure, thereby distributing loads in distinct ways. Patterns such as grid, cubic, honeycomb, and gyroid provide high tensile and compressive strength, along with good load distribution in critical structural areas [21][22]. Triangular patterns perform well in impact tests due to their superior energy absorption capabilities. Honeycomb and hexagonal patterns are recognized for their high elastic modulus, making them suitable for applications that require high energy absorption [23]. Not only do they significantly influence mechanical strength, but material efficiency and printing time are also closely related. Grid patterns print faster and use less material. Gyroid or honeycomb patterns are more complex and take longer. The selection of infill patterns is not merely aesthetic but an essential part of the internal engineering of the printed structure. Its selection must consider the type of forces acting on it, material

efficiency, printing time, and the final application of the printed product.

Another critical parameter in the 3D printing process is layer height, which significantly affects the mechanical performance and surface quality of printed components. A smaller layer height has been shown to enhance both tensile strength and interlayer adhesion, primarily due to the increased contact area between adjacent layers that promotes better bonding during deposition [24]. In addition to mechanical benefits, a reduced layer height contributes to improved surface finish, resulting in smoother textures and finer resolution of printed features. This parameter also plays a pivotal role in controlling dimensional accuracy, particularly in terms of vertical height and angular geometry. Empirical findings suggest that lower layer heights are associated with minimized dimensional deviations, thereby enhancing the geometric fidelity of the final print [25].

Moreover, chamber temperature is another influential variable that significantly determines the quality, mechanical integrity, and dimensional precision of the printed part, especially for semi-crystalline and amorphous thermoplastic polymers such as ABS, polypropylene, and Polyether Ether Ketone (PEEK). Maintaining a uniformly high ambient temperature within the printing chamber, typically 60–100 °C, is essential to mitigate common defects, such as warping, shrinkage, and internal stress formation. A controlled thermal environment facilitates homogeneous heat distribution, which in turn improves layer fusion, reduces thermal gradients, and minimizes the risk of structural porosity and microcracking [26], [27]. This thermal stability ultimately contributes to the dimensional stability and mechanical reliability of the printed component.

The combination of these parameters not only affects the geometric dimensions of the printed product but also significantly affects mechanical properties, particularly tensile strength and elongation. Many studies have mentioned the influence of each parameter individually, but there is still a lack of systematic approaches to identify the most influential parameters quantitatively [18–22]. This makes the printing optimization process a trial-and-error process, wasting time and materials.

Unfortunately, the relationship between these parameters is complex and not always linear, making it difficult to predict. Therefore, a scientific and systematic approach is needed to understand the extent to which each parameter affects mechanical properties, both individually and interactively, so that the printing process can be optimized with greater precision. The need for static and experimental analysis becomes essential. In this study, a scientific approach using the Taguchi Method to design experiments will be applied. It is hoped that the results of this research will be helpful in efforts to consistently improve print quality using ABS material as the printing material. Furthermore, another significant hope is that it can serve as the basis for developing an "ABS printing standard" based on experimental data.

2 Research methodology

This research was conducted using a systematic framework to achieve results in line with the research objectives. To answer the research questions described above, the following research stages were carried out in sequence, as shown in Fig. 1.

2.1 Printing parameters and material

This process starts with designing a 3D model using CAD software. Then, the 3D model is fed into the CreatWare slicer software. Its purpose is to convert the 3D model into G-code. Using the same slicer, the parameters specified in Table 1 are applied.

With its excellent strength and chemical resistance, ABS is the ideal filament material. ABS has better compression and thermal distortion characteristics than PLA [2]. All specimen configurations will be manufactured according to the parameters outlined in Table 1. To ensure test results are accurate, all specimens will be made from the same spool.

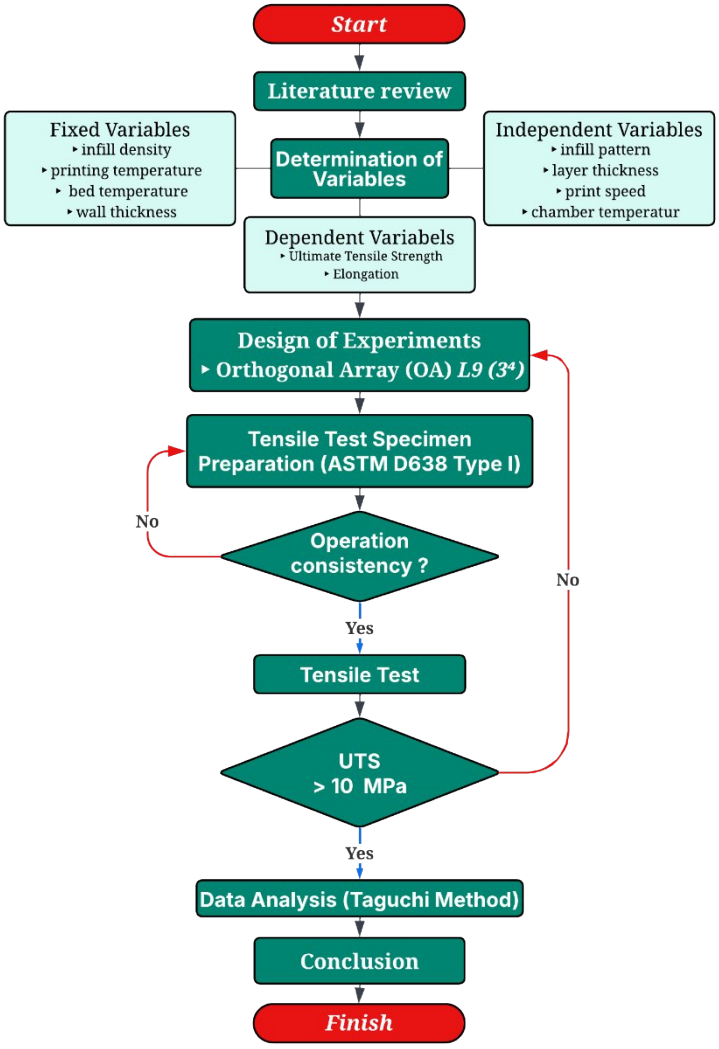

Fig. 1. Research flow chart

Table 1. Printing parameters of the testing specimens

Printing Parameters	Values	Unit
Nozzle diameter	0.4	mm
Nozzle temperature	260	℃
Bed temperature	95	℃
Shell thickness	0.8	mm
Infill density	60	%

There are many parameter configuration options available in slicing software. For example, among infill shape parameters, standard options include rectilinear, grid, triangular, honeycomb, cubic, and gyroid. All these infill shapes are designed to create lightweight structures while maintaining good strength. However, in this study, only the Gyroid, Grid, and Cubic infill shapes will be examined (Fig. 2). This selection is based on their better performance compared to other infill shapes [2][33][34]. The other independent variables used are shown in Table 2.

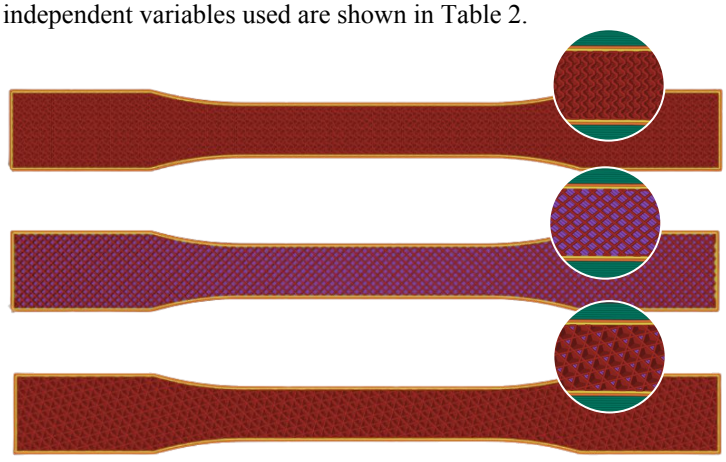

Fig. 2. Variety of infill pattern types from top to bottom: Gyroid, grid, and cubic

Table 2. Independent parameters and their levels

Parameters	Levels			Unit
	1	2	3	
Infill pattern	Gyroid	Grid	Cubic	-
Layer thickness	0.10	0.15	0.20	mm
Print speed	50	65	80	mm/s
Chamber temperature	40	50	60	℃

2.2 Design of the experiment

To obtain a combination of variables that yields the best tensile strength and elongation while minimizing the number of trials without sacrificing important information, the experimental design uses an L9(34) orthogonal array, as presented in Table 3. In this study, there were four independent parameters, each with three levels. A total of nine experimental combinations are shown in Table 3. This design aims to minimize the possibility of incorrect conclusions and reduce the influence of confounding variables.

Table 3. L9(3^4) orthogonal array

Configurations	Infill pattern	Layer thickness (mm)	Print speed (mm/s)	Chamber Temp. (°C)
1	Gyroid	0.10	50	40
2	Gyroid	0.15	65	50
3	Gyroid	0.20	80	60
4	Grid	0.10	65	60
5	Grid	0.15	80	40
6	Grid	0.20	50	50
7	Cubic	0.10	80	50
8	Cubic	0.15	50	60
9	Cubic	0.20	65	40

2.3 Specimen preparations

ASTM D368 is used as the standard test method for tensile properties of plastics, with plate dimensions as shown in Fig. 3. Then, specimens are manufactured using a CreatBot 3D printer with parameters as specified previously (Fig. 4). Next, the specimens will proceed to the tensile testing stage.

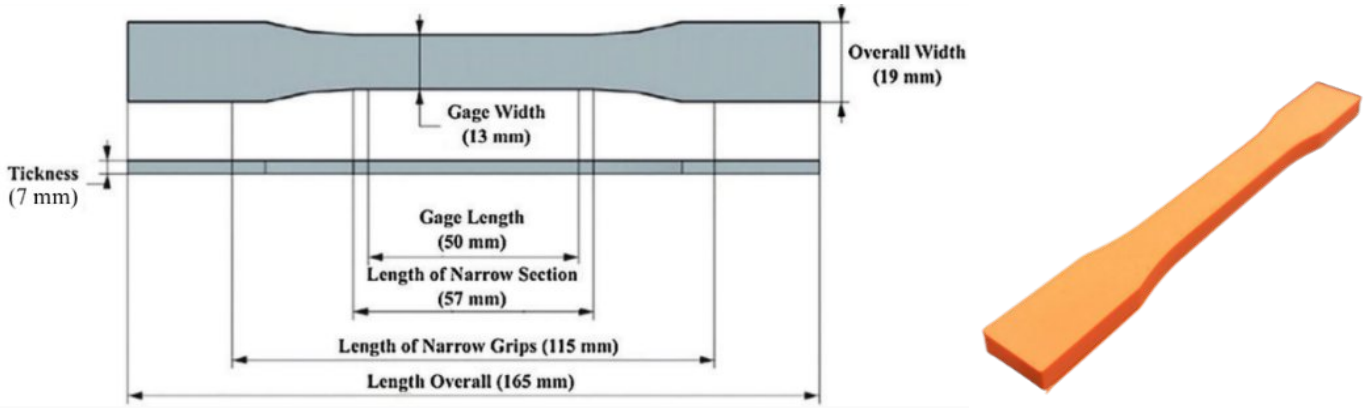

Fig. 3. Type I tensile strength test specimen according to ASTM D638

Fig. 4. CreatBot D1000 3D printer

2.4 Testing setup

Tensile testing was performed using a Tensilon RTI-1310 UTM machine. Specimens were placed consistently in the exact location for each test. The setup was performed in advance to set the test conditions. Specimen dimensions were input into the machine, and the moving speed was set at 10 mm/min, with a load cell of 5000 N. Actual settings can be seen in Fig. 5.

Fig. 5. UTM Tensilon RTI-1310 tensile testing machine

2.5 Taguchi method

To ensure analytical accuracy and reliability, the experimental data were processed using statistical software. The Taguchi method was employed to evaluate the effect of each parameter, both individually and in interaction with others. This method effectively identifies the most influential factors affecting the response

characteristics of 3D-printed specimens. The Taguchi approach involves analyzing the signal-to-noise (S/N) ratio, which quantifies the relative impact of controllable factors (the signal) versus uncontrollable or random variations (noise). A higher S/N ratio reflects greater process stability and more optimal outcomes [35].

Additionally, an Analysis of Variance (ANOVA) was conducted to determine the statistical significance of each parameter with respect to the measured mechanical properties, namely Ultimate Tensile Strength (UTS) and elongation. This multifactorial statistical approach includes the computation of degrees of freedom, sum of squares, mean squares, F-ratios, and P-values to rigorously assess the contribution and relevance of each factor within the experimental design framework [19]. The combined application of S/N ratio analysis and ANOVA offers a comprehensive evaluation of parameter effects and supports evidence-based decision-making for process optimization.

3 Results and discussion

The initial data obtained is the consistent percentage of the operation, which will be discussed in a subsection. This data serves as a basis for determining whether the operation's consistent value is as expected. If so, it will proceed to the tensile testing stage. The results of the tensile testing and elongation for the nine multi-parameter configurations are presented in Table 4. Next, the data processing for identifying the parameters most influential on tensile strength and elongation will be discussed.

Table 4. Tensile test results with multi-parameter configuration

Conf.	UTS (MPa)	Elongation (%)	Max. load (N)	S/NR A (dB)	S/NR B (dB)
1	13.934	5.096	1268	22.88	14.14
2	13.156	6.347	1197.2	22.38	16.05
3	14.218	5.652	1293.9	23.05	15.04
4	12.071	3.478	1098.5	21.63	10.82
5	10.138	4.069	922.55	20.11	12.19
6	12.696	4.500	1155.3	22.07	13.06
7	15.305	5.165	1392.8	23.69	14.26
8	15.670	4.556	1426.0	23.90	13.17
9	15.752	4.552	1433.4	23.94	13.16

3.1 Operation consistency

To minimize the risk of errors during testing, five identical tensile specimens were tested. Variations in the cubic infill pattern with a layer height of 0.20 mm, a print speed of 65 mm/s, and a chamber temperature of 40°C were used as samples to assess the consistency of specimen printing. This method was applied to maintain process consistency [34]. Thus, the difference in the maximum load that each specimen can withstand during the tensile test is only slight or insignificant.

With the same configuration, specimen number 1 had the highest maximum load value of 1433.4 N (Fig. 6). Conversely, specimen number 2 has the lowest value of 1390.3 N. This test resulted in a 3% difference between the two values. This indicates that the results of printing specimens with a 3D printer are sufficiently consistent. Therefore, the next step, tensile testing of each specimen, can proceed.

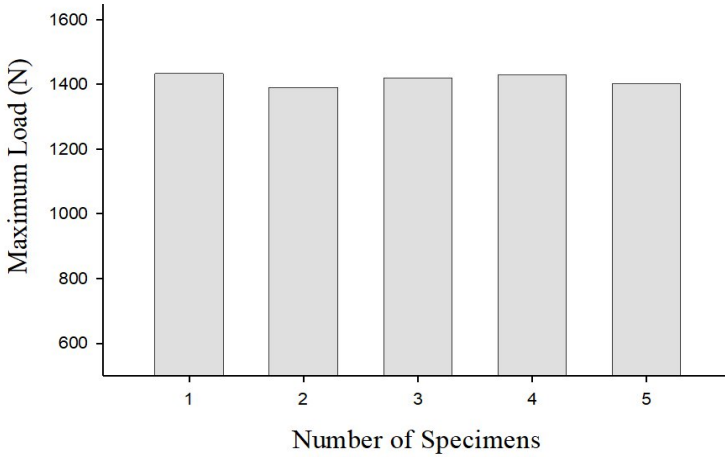

Fig. 6. Maximum point load value for each specimen

3.2 Tensile test results

From Table 4, we can see that the UTS value is possessed by configuration nine at 15.752 MPa, and the lowest is configuration five at 10.138 MPa. The highest elongation value is in configuration two at 6.34%, and the lowest is in configuration four at 3.478%. These results indicate significant differences between configurations. The elongation value is essential to note, as the material is planned to be widely used as a structural component in future UAV developments.

Table 4 also presents the results of multi-parameter S/N ratio calculations relative to response parameters (UTS and elongation). Configurations 8 and 9 have the highest S/N ratio values for UTS (SNR A). Meanwhile, the highest S/N ratio value for elongation (SNR B) is found in configuration 2. This indicates that these configurations have good resistance to variability or disturbances, resulting in more stable and reliable test results [35].

3.3 The Signal-to-Noise (SN) ratio response

To analyze the test data results in more depth, the average S/N ratio was calculated to find the most influential level for each parameter. The first step was to estimate the average S/N ratio per level, compute the delta, compile the ranks, and determine the optimal level (the parameter with the highest S/N value). Table 5 shows that the most influential parameter on UTS is the infill pattern ($\Delta = 2.57$). The most influential level for each parameter is 23.85 for level 3 in the infill pattern parameter (bolded number), similarly 23.03 for layer thickness, and 22.86 for chamber temperature. Meanwhile, the highest print speed is at level 1, with a value of 22.95.

Table 5. Mean S/N ratio response values for each control parameter relative to the UTS value (higher is better)

Level	Infill pattern	Layer thickness	Print speed	Chamber temperature
1	22.77	22.74	**22.95**	22.32
2	21.28	22.13	22.65	22.72
3	**23.85**	**23.03**	22.29	**22.86**
Delta	2.57	0.89	0.66	0.55
Rank	1	2	3	4

Fig. 7 shows the mean S/N ratio values for each level of the four independent parameters. The assessment was based on the principle of larger is better, which is commonly used in optimization. The parameter with the most significant effect on the UTS value, according to this graph, was the infill pattern, which had the most extensive range of S/N ratios. In contrast, chamber temperature had the least effect.

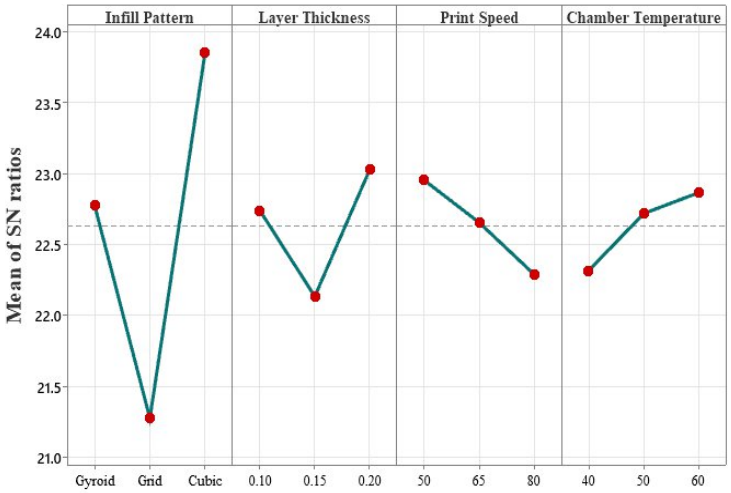

Fig. 7. Presents the mean S/N ratio plotted against UTS, where a higher value indicates better performance

Table 6 shows that the infill pattern has the most significant effect on elongation ($\Delta = 3.05$), consistent with the UTS response. However, in the following ranking, chamber temperature becomes the second most influential parameter with a value of 1.44, followed by layer thickness and print speed.

Table 6. Mean S/N ratio response values for each control parameter relative to the elongation value (higher is better)

Level	Infill pattern	Layer thickness	Print speed	Chamber temperature
1	**15.08**	13.08	13.46	13.17
2	12.03	**13.81**	13.35	**14.46**
3	13.53	13.76	**13.83**	13.01
Delta	3.05	0.73	0.48	1.44
Rank	1	3	4	2

The signal-to-noise (S/N) ratio values are presented graphically in Fig. 8 to provide a more precise visualization of each process parameter's influence. The vertical distance between the maximum and minimum average S/N ratio values serves as an indicator of the relative contribution of each parameter to the observed elongation. A greater difference suggests a more substantial effect. Based on the graphical trend, the infill pattern and chamber temperature have the most pronounced impact on elongation, indicating their critical roles in determining the mechanical behavior of 3D-printed ABS specimens.

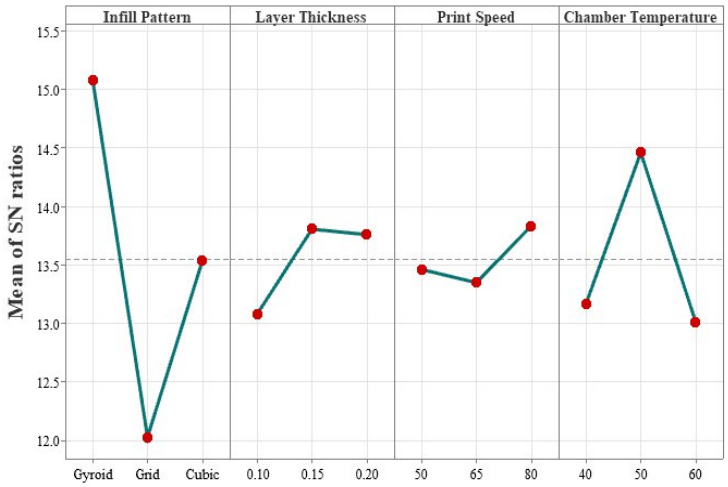

Fig. 8. Presents the mean S/N ratio plotted against elongation, where a higher value indicates better performance

3.4 ANOVA

The ANOVA calculations in this study are based on S/N ratio data that reflect UTS and elongation values, not only to optimize the mean response but also to reduce variability and improve robustness against noise. The analysis results are presented in Table 7 for the S/N ratio against the UTS response value and Table 8 for the S/N ratio against the elongation response value below. Tables 7 and 8 show that the error value is zero, indicating no residual errors. Such conditions may arise when using a Taguchi design with a 34 configuration. For comparison, Darsin M. and colleagues [36] also reported no errors when conducting experiments with a similar Taguchi design.

Table 7. ANOVA values calculated based on S/N ratio data for UTS responses

Control variable	DF	Adj SS	Adj MS	F-Value	P-Value
Infill pattern	2	10.0162	5.0081	*	*
Layer thickness	2	1.2414	0.6207	*	*
Print speed	2	0.6581	0.3290	*	*
Chamber temperature	2	0.4839	0.2419	*	*
Error	0	*	*		
Total	8	12.3996			

Table 8. ANOVA values calculated based on S/N ratio data for elongation responses

Control variable	DF	Adj SS	Adj MS	F-Value	P-Value
Infill pattern	2	13.9832	6.9916	*	*
Layer thickness	2	0.9938	0.4969	*	*
Print speed	2	0.3858	0.1929	*	*
Chamber temperature	2	3.7812	1.8906	*	*
Error	0	*	*		
Total	8	19.1440			

3.5 Percentage of contribution

The extent to which each control parameter influences the response variable can be quantified using a percentage contribution analysis. This method involves calculating the proportion of the total Sum of Squares (SS) attributable to each factor relative to the total SS obtained from the ANOVA. The resulting ratio is multiplied by 100 to express the contribution as a percentage, enabling a comparative evaluation of each parameter's significance. The detailed outcomes of this calculation, including the respective contributions of all examined factors, are presented in Table 9.

Table 9. Percentage contribution for control variables UTS and elongation

Parameters	Percentage of contribution (ρ)	
	UTS	Elongation
Infill pattern	80.78%	73.16%
Layer thickness	10.01%	5.20%
Print speed	5.31%	2.02%
Chamber temperature	5.31%	19.78%
Error	0%	0%
Total	100%	100%

3.6 Discussion of parameter effects

3.6.1 Infill pattern

In terms of tensile testing results, specimens with a cubic infill pattern had the highest and most stable UTS values, followed by those with a gyroid and a grid pattern. The cubic pattern has a three-dimensional interlocking structure that distributes load evenly throughout the specimen volume, enabling it to withstand tensile forces more effectively and to produce high, stable UTS values. The cubic structure also tends to produce better interlayer bonding, reducing stress concentration and the risk of delamination [37].

Compared to other parameters, the infill pattern contributes 80.78% of the total contribution to the UTS value and 73.16% to the elongation value. The high influence on UTS is supported by the fact that this parameter significantly controls the cross-sectional area and effective load distribution. UTS is very sensitive to changes in the internal structure pattern because the infill structure directly determines the path of tensile stress distribution. Meanwhile, as the infill structure becomes stronger (cubic or gyroid) or denser, this enhances stiffness and tensile strength but reduces elongation because the structure becomes stiffer and less flexible. Therefore, the percentage contribution to elongation decreases to 73.16%, though it remains the highest value compared to other parameters [38].

3.6.2 Layer thickness

An unusual phenomenon was observed in this control parameter. Previous studies [21][24][25][39] concluded that lower layer thickness would increase UTS because a greater number of layers results in a more uniform stress distribution. However, in this study, the highest average S/N ratio relative to UTS occurred at level 3 (Table 5), which is inconsistent with previous research. The authors suggest that excessively thin thicknesses may also cause warping and thermal deformation if chamber temperature is not controlled, which is closely related to the chamber temperature control parameter. The relationship between the two parameters requires further investigation in subsequent studies.

Meanwhile, the contribution to the elongation value is not too significant, at 5.20%. This occurs because thicker layers produce more ductile, flexible parts, allowing greater plastic deformation before failure. Meanwhile, in lower layers, despite strong adhesion, the material tends to be more rigid and brittle, causing elongation to decrease [40].

3.6.3 Print speed

Print speed, defined as the rate at which the nozzle moves during printing, influences the mechanical properties of 3D-printed components, particularly tensile strength. Based on the percentage contribution analysis, this parameter accounts for 5.31% of the

variation in UTS and 2.02% of the variation in elongation. Although these values indicate a relatively minor influence compared to other process parameters, the effect of print speed is still noteworthy. An increase in print speed tends to reduce the UTS of ABS specimens, which is attributed to under-extrusion. This condition often leads to the formation of micro-voids and weak interlayer adhesion, ultimately compromising the structural integrity of the printed part. Nonetheless, the overall influence of print speed remains statistically insignificant when compared to the more dominant factors in the study.

3.6.4 Chamber temperature

As shown in Table 9, the contribution value of this parameter is 5.31% to UTS and 19.78% to the elongation value. Higher chamber temperatures contribute to a decrease in internal porosity and an increase in interlayer bonding. The significant influence on elongation values makes it the second-highest contributor after infill pattern due to strong adhesion, minimal porosity, and slower layer cooling, allowing for greater plastic deformation before cracking occurs [41].

The results of this study indicate that optimizing the infill pattern and chamber temperature can significantly enhance the tensile strength of 3D-printed ABS materials. This improvement is highly relevant to the development of UAV structures, which require lightweight materials with high mechanical reliability. The enhanced tensile performance achieved through appropriate process parameter selection suggests that AM can be effectively utilized to produce structurally dependable UAV components. Furthermore, the findings of this work provide a scientific basis for our subsequent research, which aims to evaluate the performance of ABS materials when applied to the structural spar of UAV wings under realistic loading conditions.

4 Conclusions

Each print parameter has a significant, but varying, effect on the mechanical properties of ABS. In general, the infill pattern parameter accounts for 80.78% of UTS, as the internal infill pattern significantly influences stress distribution and tensile strength. Slightly lower, the contribution to elongation is lower (73.16%) due to an increase in the contribution of the chamber temperature parameter (19.78%). Layer thickness moderately affects UTS; a thickness of 0.2 mm tends to be optimal as it produces balanced interlayer bonding. However, its effect on elongation is more complex and less significant.

Print speed is the least influential parameter on both values, UTS and elongation. Unlike chamber temperature, this parameter significantly affects both. UTS increases due to reduced porosity and enhanced interlayer bonding, while elongation rises due to the release of internal stress during slow cooling. The ideal temperature range is 50–60°C.

References

[1] A. Malim, N. Mourousias, B. G. Marinus, and T. De Troyer, "Structural Design of a Large-Scale 3D-Printed High-Altitude Propeller: Methodology and Experimental Validation," *Aerospace*, vol. 10, no. 3, p. 256, Mar. 2023, doi: 10.3390/aerospace10030256.

[2] H. B. Ali, J. K. Oleiwi, and F. M. Othman, "Compressive and Tensile Properties of ABS Material as a Function of 3D Printing Process Parameters," *Revue des composites et des matériaux avancés*, vol. 32, no. 3, pp. 117–123, Jun. 2022, doi: 10.18280/rcma.320302.

[3] F. Ahmed, J. C. Mohanta, A. Keshari, and P. S. Yadav, "Recent Advances in Unmanned Aerial Vehicles: A Review," *Arab J Sci Eng*, vol. 47, no. 7, pp. 7963–7984, Jul. 2022, doi: 10.1007/s13369-022-06738-0.

[4] N. A. Ahmed and J. R. Page, "Manufacture of an Unmanned Aerial Vehicle (UAV) for Advanced Project Design Using 3D Printing Technology," *Applied Mechanics and Materials*, vol. 397–400, pp. 970–980, Sep. 2013, doi: 10.4028/www.scientific.net/AMM.397-400.970.

[5] S. Easter, J. Turman, D. Sheffler, M. Balazs, and J. Rotner, "Using advanced manufacturing to produce unmanned aerial vehicles: a feasibility study," T. Pham, M. A. Kolodny, and K. L. Priddy, Eds., May 2013, p. 874204. doi: 10.1117/12.2027616.

[6] M. Akkamış and S. Çalışkan, "İnsansız Hava Araçları ve Tarımsal Uygulamalarda Kullanımı," *Türkiye İnsansız Hava Araçları Dergisi*, vol. 2, no. 1, pp. 8–16, 2020.

[7] J.-P. Kruth, M. C. Leu, and T. Nakagawa, "Progress in Additive Manufacturing and Rapid Prototyping," *CIRP Annals*, vol. 47, no. 2, pp. 525–540, 1998, doi: 10.1016/S0007-8506(07)63240-5.

[8] J. Mogan, L. Sandanamsamy, N. A. Halim, W. S. W. Harun, K. Kadirgama, and D. Ramasamy, "A review of FDM and graphene-based polymer composite," *IOP Conf Ser Mater Sci Eng*, vol. 1078, no. 1, p. 012032, Feb. 2021, doi: 10.1088/1757-899X/1078/1/012032.

[9] A. Mosaddek, H. K. R. Kommula, and F. Gonzalez, "Design and Testing of a Recycled 3D Printed and Foldable Unmanned Aerial Vehicle for Remote Sensing," in *2018 International Conference on Unmanned Aircraft Systems (ICUAS)*, 2018, pp. 1207–1216. doi: 10.1109/ICUAS.2018.8453284.

[10] E. Atzeni, L. Iuliano, P. Minetola, and A. Salmi, "Redesign and cost estimation of rapid manufactured plastic parts," *Rapid Prototyp J*, vol. 16, no. 5, pp. 308–317, Aug. 2010, doi: 10.1108/13552541011065704.

[11] J. Mieloszyk, A. Tarnowski, M. Kowalik, R. Perz, and W. Rzadkowski, "Preliminary design of 3D printed fittings for UAV," *Aircraft Engineering and Aerospace Technology*, vol. 91, no. 5, pp. 756–760, May 2019, doi: 10.1108/AEAT-07-2018-0182.

[12] S. K. Moon, Y. E. Tan, J. Hwang, and Y.-J. Yoon, "Application of 3D printing technology for designing light-weight unmanned aerial vehicle wing structures," *International Journal of Precision Engineering and Manufacturing-Green Technology*, vol. 1, no. 3, pp. 223–228, Jul. 2014, doi: 10.1007/s40684-014-0028-x.

[13] S. Brischetto, C. G. Ferro, R. Torre, and P. Maggiore, "3D FDM production and mechanical behavior of polymeric sandwich specimens embedding classical and honeycomb cores," *Curved and Layered Structures*, vol. 5, no. 1, pp. 80–94, Apr. 2018, doi: 10.1515/cls-2018-0007.

[14] H. Klippstein, H. Hassanin, A. Diaz De Cerio Sanchez, Y. Zweiri, and L. Seneviratne, "Additive Manufacturing of Porous Structures for Unmanned Aerial Vehicles Applications," *Adv Eng Mater*, vol. 20, no. 9, Sep. 2018, doi: 10.1002/adem.201800290.

[15] Ahmed. O. MohamedZain, H. Chua, K. Yap, P. Uthayasurian, and T. Jiehan, "Novel Drone Design Using an Optimization Software with 3D Model, Simulation, and Fabrication in Drone Systems Research," *Drones*, vol. 6, no. 4, p. 97, Apr. 2022, doi: 10.3390/drones6040097.

[16] I. Palinkas, J. Pekez, E. Desnica, A. Rajic, and D. Nedelcu, "Analysis and Optimization of UAV Frame Design for Manufacturing from Thermoplastic Materials on FDM 3D Printer," *Materiale Plastice*, vol. 58, no. 4, pp. 238–249, Jan. 2022, doi: 10.37358/MP.21.4.5549.

[17] T. Gulo, D. Mardiyana, and D. I. Sumarno, "Analysis of Print Speed Variations Effect and Nozzle Temperature on the Tensile Strength of 3D Printed TPU-95A Products," *Jurnal Konversi Energi dan Manufaktur*, pp. 53–60, Jan. 2025, doi: 10.21009/JKEM.10.1.6.

[18] J. H. S. Almeida, S. Jayaprakash, K. Kolari, J. Kuva, K. Kukko, and J. Partanen, "The role of printing parameters on the short beam strength of 3D-printed continuous carbon fibre reinforced epoxy-PETG composites," *Compos Struct*, vol.

337, p. 118034, Jun. 2024, doi: 10.1016/j.compstruct.2024.118034.

[19] A. R. Muhammad, R. R. Sakura, D. Dwilaksana, Sumarji, and M. Trifiananto, "Layer Height, Temperature Nozzle, Infill Geometry and Printing Speed Effect on Accuracy 3D Printing PETG," *R.E.M. (Rekayasa Energi Manufaktur) Jurnal*, vol. 7, no. 2, pp. 81–88, Nov. 2022, doi: 10.21070/r.e.m.v7i2.1649.

[20] M. Lei, Q. Wei, M. Li, J. Zhang, R. Yang, and Y. Wang, "Numerical Simulation and Experimental Study the Effects of Process Parameters on Filament Morphology and Mechanical Properties of FDM 3D Printed PLA/GNPs Nanocomposite," *Polymers (Basel)*, vol. 14, no. 15, p. 3081, Jul. 2022, doi: 10.3390/polym14153081.

[21] A. P. Agrawal, V. Kumar, J. Kumar, P. Paramasivam, S. Dhanasekaran, and L. Prasad, "An investigation of combined effect of infill pattern, density, and layer thickness on mechanical properties of 3D printed ABS by fused filament fabrication," *Heliyon*, vol. 9, no. 6, p. e16531, Jun. 2023, doi: 10.1016/j.heliyon.2023.e16531.

[22] J. M. Cañero-Nieto, R. J. Campo-Campo, I. Díaz-Bolaño, E. A. Ariza-Echeverri, C. E. Deluque-Toro, and J. F. Solano-Martos, "Infill pattern strategy impact on the cross-sectional area at gauge length of material extrusion 3D printed polylactic acid parts," *J Intell Manuf*, Feb. 2025, doi: 10.1007/s10845-025-02579-4.

[23] S. Mahović Poljaček, D. Donevski, T. Tomašegović, U. Vrabič Brodnjak, and M. Leskovšek, "Mechanical Properties of 3D-Printed PLA Structures Observed in Framework of Different Rotational Symmetry Orders in Infill Patterns," *Symmetry (Basel)*, vol. 17, no. 3, p. 466, Mar. 2025, doi: 10.3390/sym17030466.

[24] J. R. Stojković *et al.*, "An Experimental Study on the Impact of Layer Height and Annealing Parameters on the Tensile Strength and Dimensional Accuracy of FDM 3D Printed Parts," *Materials*, vol. 16, no. 13, p. 4574, Jun. 2023, doi: 10.3390/ma16134574.

[25] G. Tattimbetova, G. Zhetessova, J. Škamat, and A. Mateshov, "Impact of Layer Height on Dimensional Accuracy in FDM 3D Printing," in *2024 IEEE 6th International Symposium on Logistics and Industrial Informatics (LINDI)*, IEEE, Oct. 2024, pp. 183–188. doi: 10.1109/LINDI63813.2024.10820411.

[26] A. Kholil, E. A. Syaefudin, A. Juniar, M. K. Rohim, and S. T. Dwiyati, "Simulation of temperature distribution in 3D printing heated chamber on orientation and temperature variations with ABS material," *J Phys Conf Ser*, vol. 2596, no. 1, p. 012007, Sep. 2023, doi: 10.1088/1742-6596/2596/1/012007.

[27] M. Spörk *et al.*, "The consequences of different printing chamber temperatures in extrusion-based additive manufacturing," 2018. [Online]. Available: https://api.semanticscholar.org/CorpusID:140029746

[28] S. Rouf, A. Raina, M. Irfan Ul Haq, N. Naveed, S. Jeganmohan, and A. Farzana Kichloo, "3D printed parts and mechanical properties: Influencing parameters, sustainability aspects, global market scenario, challenges and applications," *Advanced Industrial and Engineering Polymer Research*, vol. 5, no. 3, pp. 143–158, Jul. 2022, doi: 10.1016/j.aiepr.2022.02.001.

[29] V. Cojocaru, D. Frunzaverde, C.-O. Miclosina, and G. Marginean, "The Influence of the Process Parameters on the Mechanical Properties of PLA Specimens Produced by Fused Filament Fabrication—A Review," *Polymers (Basel)*, vol. 14, no. 5, p. 886, Feb. 2022, doi: 10.3390/polym14050886.

[30] J. A. Afonso, J. L. Alves, G. Caldas, B. P. Gouveia, L. Santana, and J. Belinha, "Influence of 3D printing process parameters on the mechanical properties and mass of PLA parts and predictive models," *Rapid Prototyp J*, vol. 27, no. 3, pp. 487–495, Apr. 2021, doi: 10.1108/RPJ-03-2020-0043.

[31] M. Benamira, N. Benhassine, A. Ayad, and A. Dekhane, "Investigation of printing parameters effects on mechanical and failure properties of 3D printed PLA," *Eng Fail Anal*, vol. 148, p. 107218, Jun. 2023, doi: 10.1016/j.engfailanal.2023.107218.

[32] D. Lee and G.-Y. Wu, "Parameters Affecting the Mechanical Properties of Three-Dimensional (3D) Printed Carbon Fiber-Reinforced Polylactide Composites," *Polymers (Basel)*, vol. 12, no. 11, p. 2456, Oct. 2020, doi: 10.3390/polym12112456.

[33] J. Podroužek, M. Marcon, K. Ninčević, and R. Wan-Wendner, "Bio-Inspired 3D Infill Patterns for Additive Manufacturing and Structural Applications," *Materials*, vol. 12, no. 3, p. 499, Feb. 2019, doi: 10.3390/ma12030499.

[34] B. Pernet, J. K. Nagel, and H. Zhang, "Compressive Strength Assessment of 3D Printing Infill Patterns," *Procedia CIRP*, vol. 105, pp. 682–687, 2022, doi: 10.1016/j.procir.2022.02.114.

[35] C. M. Ferreira, C. M. S. Vicente, M. Sardinha, M. Leite, and L. Reis, "Characterization of 3D printed ABS specimens under static and cyclic torsional loadings," *Procedia Structural Integrity*, vol. 34, pp. 205–210, 2021, doi: 10.1016/j.prostr.2021.12.030.

[36] M. Darsin, R. R. Mauludy, I. Hardiatama, B. A. Fachri, M. E. Ramadhan, and D. Parningotan, "Analysis of the effect 3D printing parameters on tensile strength using Copper-PLA filament," *SINERGI*, vol. 26, no. 1, p. 99, Feb. 2022, doi: 10.22441/sinergi.2022.1.013.

[37] M. Rizwee and D. Kumar, "Contribution of geometrical infill pattern on mechanical behaviour of 3D manufactured polylactic acid specimen: Experimental and numerical analysis," *Progress in Rubber, Plastics and Recycling Technology*, vol. 41, no. 3, pp. 331–351, Aug. 2025, doi: 10.1177/14777606241281614.

[38] M. Daly, M. Tarfaoui, M. Bouali, and A. Bendarma, "Effects of Infill Density and Pattern on the Tensile Mechanical Behavior of 3D-Printed Glycolyzed Polyethylene Terephthalate Reinforced with Carbon-Fiber Composites by the FDM Process," *Journal of Composites Science*, vol. 8, no. 4, p. 115, Mar. 2024, doi: 10.3390/jcs8040115.

[39] C. Abeykoon, P. Sri-Amphorn, and A. Fernando, "Optimization of fused deposition modeling parameters for improved PLA and ABS 3D printed structures," *International Journal of Lightweight Materials and Manufacture*, vol. 3, no. 3, pp. 284–297, Sep. 2020, doi: 10.1016/j.ijlmm.2020.03.003.

[40] M. N. Ahmad and A. Yahya, "Effects of 3D Printing Parameters on Mechanical Properties of ABS Samples," *Designs (Basel)*, vol. 7, no. 6, p. 136, Nov. 2023, doi: 10.3390/designs7060136.

[41] K. Q. Nguyen *et al.*, "Effect of in Situ Thermal Treatment on ABS Parts produced by Fused Deposition Modeling (FDM)," Sep. 17, 2024. doi: 10.21203/rs.3.rs-4921521/v1.